Data-driven characterization of pedestrian flows

Marija Nikolić * Michel Bierlaire *

August 15, 2016

Report TRANSP-OR 160815
Transport and Mobility Laboratory
School of Architecture, Civil and Environmental Engineering
Ecole Polytechnique Fédérale de Lausanne
transp-or.epfl.ch

*Transport and Mobility Laboratory, School of Architecture, Civil and Environmental Engineering, École Polytechnique Fédérale de Lausanne, Switzerland,
{marija.nikolic, michel.bierlaire}@epfl.ch

Abstract

We propose a novel approach to pedestrian flow characterization. The definitions of density, flow and velocity existing in the literature are extended through a data-driven spatio-temporal discretization framework. The framework is based on three-dimensional Voronoi diagrams. The new definitions are (i) independent from an arbitrarily chosen discretization; (ii) appropriate for the multi-directional composition of pedestrian traffic; (iii) able to reflect the heterogeneity of the pedestrian population; and (iv) applicable to pedestrian trajectories described either analytically or as a sample of points. Synthetic data is used to empirically investigate the performance of the approach and to illustrate its advantages.

Keywords: pedestrian flow, time and space discretization, three-dimensional Voronoi diagrams, individual trajectories, robust indicators

1 Introduction

Research on pedestrian traffic has received growing attention during the last decades due to its importance in many aspects: planning of walking facilities under regular and safety-critical circumstances, operations in large events, description of congestion, etc. To increase insights into pedestrian movements, different empirical studies were conducted and reported in the literature (Hoogendoorn and Daamen, 2004, Helbing et al., 2005). The empirical observations have inspired a number of theories and models that are utilized to describe and predict pedestrian movement (Duives et al., 2013, Hänseler et al., 2014, Hoogendoorn et al., 2014).

The fundamental variables used to observe and to model the traffic of pedestrians are density (k), flow (q) and velocity (v). *Density* is expressed as the number of pedestrians per unit of space at a given moment in time; *flow* is interpreted as the number of pedestrians per unit of time and per unit of length; *velocity* is expressed in meters per unit of time. Several definitions of these variables are proposed in the literature (Duives et al., 2015, Zhang, 2012). However, little concern is dedicated to the nature of spatial and temporal discretization underlying the definitions. The basic issue is that there are many possible ways to discretize continuous space and time for the purpose of defining traffic variables. Yet, studies normally report the analysis for one particular discretization scheme whose choice is often arbitrary.

The aim of this study is the derivation of a discretization framework that is independent from arbitrarily chosen values, and that results in a realistic and robust pedestrian flow characterization. We propose to adjust the discretization to the data itself using a data-driven approach. The approach is based on spatio-temporal Voronoi diagrams designed through the utilization of pedestrian trajectories.

The structure of the paper is as follows. A review of related research from the literature is provided in Section 2. Section 3 provides a formal introduction of the basic elements involved in our analysis. Section 4 describes the proposed methodology for the derivation of the spatio-temporal discretization framework. Based on this framework, we derive the definitions of the pedestrian traffic variables, that is density, flow and velocity. Section 5 empirically illustrates the performance of the approach by using synthetic data. Finally, Section 6 summarizes the outcomes of the proposed methodology and determines future research directions.

2 Literature review

The issue of discretization is well recognized in geography (Openshaw, 1984, Çöltekin et al., 2011) and dynamic systems (Beck and Roepstorff, 1987). The research from the field of geography have demonstrated that the results of any spatio-temporal analysis depend severely on the underlying discretization. The problem appears in two dimensions, space and time (known as Modifiable Areal Unit Problem and Modifiable Temporal Unit Problem). For instance, analysis of data using grid-based spatial discretization differs from analysis performed using hexagon cells. Similarly, temporal discretization may distort or exaggerate the actual temporal pattern existing in data if it is based on an arbitrary choice. It is therefore essential that the discretization rely on a meaningful basis relevant for the purpose of the study. The definition of discretization scheme has to precede any attempt to define characteristics based on it.

This section first focuses on vehicular traffic characterization, that is relevant for pedestrian as well. However, for most applications in pedestrian flow theory the definitions derived in the field of vehicular traffic can not be directly used. In comparison to roadways where vehicular flow is regulated and separated by directions, the lack of strict rules for pedestrians to follow allows them to occupy any part of the walkable area and to move in a multi-directional fashion. We then present the approaches specific to pedestrian traffic characterization and their comparison.

2.1 Vehicular traffic

The most general and widely used definitions of vehicular traffic variables are proposed by Edie (1963). The definitions are derived based on the trajectories of vehicles $i = 1, ..., N$ in the time-space region A. The shape of the region A is

usually rectangular with duration dt and length dx. The definitions are given as

$$k(A) = \frac{\sum_{i=1}^{N} t_i}{dxdt}, \tag{1}$$

$$q(A) = \frac{\sum_{i=1}^{N} x_i}{dxdt}, \tag{2}$$

$$v(A) = \frac{\sum_{i=1}^{N} x_i}{\sum_{i=1}^{N} t_i}, \tag{3}$$

where t_i and x_i are the time spent by vehicle i, respectively the distance traversed by vehicle i in the region A. This approach is applicable to any time-space domain of interest and provides consistent results in observations and modeling. The determination of the shape, the size and the placement of the time-space region A is however left to the modeler.

Some authors propose a "vehicle-based" discretization (Jabari et al., 2014; Treiber and Kesting, 2013). The definitions of the indicators with this discretization are consistent with the classical definitions of Edie (1963), but with the space-time intervals chosen to fit exactly one vehicle each. Let $x_{i-1}(t)$ and $x_i(t)$ denote the positions of the leader, $i-1$, and the follower, i, at time t. The spacing is defined as $s_i(t) = x_{i-1}(t) - x_i(t)$. The density at time t is defined as the inverse of the spacing $s_i(t)$ measured at that time

$$k(x,t) = \frac{1}{s_i(t)}, \text{ for } x \in [x_i(t), x_{i-1}(t)). \tag{4}$$

Let $t_i(x)$ denote the time when vehicle i crosses position x. The time headway is defined as $h_i(x) = t_i(x) - t_{i-1}(x)$. The flow at position x is defined as the inverse of the time headway $h_i(x)$ measured at that location

$$q(x,t) = \frac{1}{h_i(x)}, \text{ for } t \in (t_{i-1}(x), t_i(x)]. \tag{5}$$

Speed is defined as the ratio between flow and density

$$v(x,t) = \frac{s_i(t)}{h_i(x)}, \text{ for } x \in [x_i(t), x_{i-1}(t)), t \in (t_{i-1}(x), t_i(x)], \tag{6}$$

and it represents a mean speed for vehicle i. This microscopic approach allows to preserve the heterogeneity of driver population.

2.2 Pedestrian traffic

In this section we first present a general description of the approaches available in the field of pedestrian traffic. Then, the theoretical and technical differences of the approaches are discussed.

2.2.1 Description of methods

One of the first approaches to pedestrian flow characterization was proposed by Fruin (1971). In this method a grid-based spatial discretization is considered and density is defined as

$$k(x, y, t) = \frac{N_A(t)}{|A|}, \text{ for } (x, y) \in A, \tag{7}$$

where A is a grid cell, $|A|$ is the area of A, and $N_A(t)$ represents the number of pedestrians present in the cell A at a specific time instant t. The instantaneous velocity of pedestrian i at t is specified using the following formulation

$$\vec{v}_i(t) = \frac{\begin{pmatrix} x_i(t_2) \\ y_i(t_2) \end{pmatrix} - \begin{pmatrix} x_i(t_1) \\ y_i(t_1) \end{pmatrix}}{t_2 - t_1}, \tag{8}$$

where $(x_i(t), y_i(t))^T$ refers to the position of pedestrian i, and t_1 and t_2 define the time instants before, respectively after time t. In general, no guidance is provided for the selection of these time instants. The velocity within the cell A is then given as the average of individual instantaneous velocities

$$\vec{v}(x, y, t) = \frac{\sum_{i=1}^{N_A} \vec{v}_i(t)}{N_A}, \text{ for } (x, y) \in A. \tag{9}$$

The flow is determined using the fundamental flow equation

$$\vec{q}(x, y, t) = k(x, y, t)\vec{v}(x, y, t). \tag{10}$$

In the rest of the paper, we refer to this method as the grid-based method (GB).

The range-based method (RB) is similar to the grid-based method (Duives et al., 2015). The difference is that a circle defined by radius r at any discrete location in space is used instead of rectangular cells.

In van Wageningen-Kessels et al. (2014) (similar to Saberi et al., 2014) the definitions of Edie (1963) are extended by studying pedestrian traffic in a three-dimensional time-space diagram A (of length dx, width dy and duration dt) with

pedestrians $i = 1, ..., N$. The density is defined as the average number of pedestrians in the region $[dx \times dy]$ during time period dt

$$k(A) = \frac{\sum_{i=1}^{N} t_i}{dxdydt}, \tag{11}$$

where t_i is the time during which pedestrian i is present in the region A. The flow is defined in x and y directions as

$$\vec{q}(A) = \begin{pmatrix} q_x(A) \\ q_y(A) \end{pmatrix} = \begin{pmatrix} \frac{\sum_{i=1}^{N} x_i}{dxdydt} \\ \frac{\sum_{i=1}^{N} y_i}{dxdydt} \end{pmatrix}, \tag{12}$$

where x_i and y_i are the distances traveled in A in direction x, respectively y by pedestrian i. The velocity in direction x (or y) is defined as the average distance traveled in x direction (or in y direction) divided by the total time spent

$$\vec{v}(A) = \begin{pmatrix} v_x(A) \\ v_y(A) \end{pmatrix} = \begin{pmatrix} \frac{\sum_{i=1}^{N} x_i}{\sum_{i=1}^{N} t_i} \\ \frac{\sum_{i=1}^{N} y_i}{\sum_{i=1}^{N} t_i} \end{pmatrix}. \tag{13}$$

At the limit $dt \to 0$, the density converges to the number of pedestrians present in $[dx \times dy]$ at a specific moment in time. At the limit $dx \to 0$ ($dy \to 0$) flow converges to the number of pedestrians per unit of time and per unit of length. In the rest of the paper, we refer to this method as the XY-T method.

Another approach is provided by Helbing et al. (2007). This method defines the characteristics at any point (x, y) by weighting the relative influence of the surrounding pedestrians using Gaussian distance-dependent weight function

$$f\left(\begin{pmatrix} x_i(t) \\ y_i(t) \end{pmatrix} - \begin{pmatrix} x \\ y \end{pmatrix} \right) = \frac{1}{\pi R^2} \exp\left(- \frac{\left\| \begin{pmatrix} x_i(t) \\ y_i(t) \end{pmatrix} - \begin{pmatrix} x \\ y \end{pmatrix} \right\|^2}{R^2} \right), \tag{14}$$

where R represents the distance up-to-which the influence of pedestrians is taken into account, and $(x_i(t), y_i(t))^T$ the location of pedestrian i. The density is defined as

$$k(x, y, t) = \sum_i f\left(\begin{pmatrix} x_i(t) \\ y_i(t) \end{pmatrix} - \begin{pmatrix} x \\ y \end{pmatrix} \right). \tag{15}$$

The velocity is given by

$$\vec{v}(x,y,t) = \frac{\sum_i \vec{v}_i(t) f\left(\begin{pmatrix} x_i(t) \\ y_i(t) \end{pmatrix} - \begin{pmatrix} x \\ y \end{pmatrix} \right)}{\sum_i f\left(\begin{pmatrix} x_i(t) \\ y_i(t) \end{pmatrix} - \begin{pmatrix} x \\ y \end{pmatrix} \right)}, \tag{16}$$

where $\vec{v}_i(t)$ is the velocity of pedestrian i at time t, which is given by (8). The flow is determined using the fundamental flow equation (10). In the rest of the paper, we refer to this method as the exponentially weighted distance method (EW).

Steffen and Seyfried (2010) propose the method in which the spatial discretization is adjusted to the data through the use of Voronoi diagrams (Okabe et al., 2000). The Voronoi space decomposition assigns a personal region A_i to each pedestrian i, in such a way that each point in the personal region is closer to i than to any other pedestrian, with respect of the Euclidean distance. The density at position (x, y) at time t is defined as

$$k(x,y,t) = \frac{1}{|A_i|}, \text{ for } (x,y) \in A_i, \tag{17}$$

where $|A_i|$ is the area of A_i. The velocity is defined based on position differences of pedestrian i between time instances t_1 and t_2

$$\vec{v}(x,y,t) = \frac{\begin{pmatrix} x_i(t_2) \\ y_i(t_2) \end{pmatrix} - \begin{pmatrix} x_i(t_1) \\ y_i(t_1) \end{pmatrix}}{t_2 - t_1}, \text{ for } (x,y) \in A_i, \tag{18}$$

where $(x_i(t), y_i(t))^T$ is the location of pedestrian i at time t. Time instances t_1 and t_2 are determined such that the effect of the swaying movement of pedestrians is reduced, which requires an extensive pre-processing of each pedestrian trajectory. The flow within an interval is defined using fractional counts obtained from Voronoi cells: half a person has passed a segment if half of the Voronoi cell has passed it. For more details we refer to Steffen and Seyfried (2010). In the rest of the paper, we refer to this method as the Voronoi-based method (VB).

There also exist headway-based approaches for the definition of density variable, such as Harmonically Weighted Mean Distance and Minimum Distance, both with or without a vision field taken into account. According to Duives et al. (2015), these approaches are not capable of providing correct and consistent estimation and are therefore excluded from the further analysis in our study.

2.2.2 Comparison of methods

A summary of general characteristics of the approaches is provided in Table 1. We first compare the approaches in terms of the scale that is considered, that is in terms of whether the characterization is defined by using the information about a single pedestrian (microscopic) or multiple pedestrians (macroscopic). Then, the analysis is made with respect to the exact way the spatial and temporal aggregation is performed at a given scale. Finally, the approaches are contrasted in terms of the type of data required to perform the characterization.

Method	Scale	Spatial aggregation		Temporal aggregation		Data type
		Unit	Assumptions	Unit	Assumptions	
XY-T	Macroscopic	Area	Shape Size Location	Interval	Duration	Trajectories
Grid-based (GB)	Macroscopic	Cell	Size Location	Interval	Duration	Trajectories Sync. sample
Range-based (RB)	Macroscopic	Circle	Radius Location	Interval	Duration	Trajectories Sync. sample
Exponentially-weighted (EW)	Macroscopic	Range	Influence function Range of influence	Interval	Duration	Trajectories Sync. sample
Voronoi-based (VB)	Microscopic	Voronoi cell	Boundary conditions	Interval	Duration	Trajectories Sync. sample

Table 1: Characteristics of the approaches

Most of the methods (XY-T, GB, RB, EW) rely on macroscopic approach. This approach does not always comply with the nature of the underlying system. Pedestrians differ in many ways (Weidmann, 1993) and studying pedestrian movement at the macroscopic level may lead to the loss of heterogeneity. Also, by using macroscopic definitions, velocity and flow vectors may cancel out if the pedestrians do not all move in the same direction. On the other hand, microscopic characterization (employed in the VB method) is able to reflect these particularities of pedestrian traffic. It is further supported by detailed movement data (at the individual level) that is more and more available due to the advances in tracking technologies (Bauer et al., 2009). The microscopic approach is characterized by higher computational burden, which becomes less problematic in the era of high-performance computers.

All the approaches have in common the arbitrary chosen temporal intervals for the specification of velocity and flow indicators. Most of them (XY-T, GB, RB, EW) additionally depend on an arbitrary spatial aggregation. These may generate noise in the data and the results may be highly sensitive to minor changes. The choice of the shape, size and locations of the spatial units in the methods XY-T, GB and RB influences the results significantly. Also, the use of fixed aggregation over time might cause large fluctuations in the indicator values when pedestrians cross the boundaries of the aggregation units. An additional level of arbitrariness is introduced when a pedestrian is exactly at the border between two units, and an

arbitrary decision must be made about what units she belongs to. Indicators obtained using the EW approach strongly depend on the radius R and, in general, on the choice of the influence function f, given by (14). The VB method of Steffen and Seyfried (2010) is the only one that addresses the issue of arbitrary aggregation in space through a data-driven approach. The spatial units in this approach are not fixed over time. Aggregation follows the trend of the data by computing Voronoi diagrams for every time step. The issue is that Voronoi diagram is potentially not enclosed. There is no clear understanding about where to put the Voronoi boundaries in directions where no other pedestrians are present. Steffen and Seyfried (2010) use a restriction of the individual cells in size ($2m^2$) to deal with this issue, which is active only for a few cells.

An analytical description of the trajectories is required for the XY-T method. Consequently, interpolation has to be used when sampled data is available, which is another source of errors. The methods GB, RB, EW and VB can be applied on trajectories described either analytically or as a sample of points. Note that these approaches require a tracking technology that produces synchronized samples. Often, the cameras used to track pedestrians in a distributed network of cameras operate with different sampling frequency or produce observations at irregular intervals. In this case not all trajectories have observations at the same time instants, which might lead to the underestimation of the indicators. It is therefore necessary to perform the interpolation of trajectories when using non-synchronized samples, before applying the methods.

The methodology proposed in this article is similar to the approach used in Jabari et al. (2014). It relies on the microscopic definitions of Edie (1963) adopted for pedestrian traffic.

3 Preliminaries

We consider a space-time representation and denote the area of interest by $\Omega \subset \mathbb{R}^3$. An orthonormal basis of this space is considered. The distance along each of the two spatial axes is expressed in meters, and the unit for time is seconds. The triplet $p = (p_x, p_y, p_t) = (x, y, t) \in \Omega$ represents a physical position (x, y) in space at a specific time t. It is assumed that Ω is convex, that is obstacle-free, and bounded.

The trajectory of pedestrian i is a curve in space and time. It is a set of points

$$\Gamma_i : \{p_i(t) | p_i(t) = (x_i(t), y_i(t), t)\}, \tag{19}$$

indexed by time t that spans the horizon of the analysis, and $x_i(t)$ and $y_i(t)$ are the coordinates of the position of pedestrian i at time t.

In practice, the analytical description of a trajectory is seldom available. Instead, the pedestrian trajectory data is collected through an appropriate tracking technology (Alahi et al., 2014; Daamen and Hoogendoorn, 2003). In this case time is discretized and the trajectory is described as a finite collection of triplets (a sample of points)

$$\Gamma_i : \{p_{is} | p_{is} = (x_{is}, y_{is}, t_s)\}, \tag{20}$$

where $s = [1, 2, ..., T_i]$ and $t_s = [t_1, t_2, ..., t_{T_i}]$ correspond to the available sample.

The speed along the continuous trajectory of pedestrian i is given by

$$v_i(t) = (x_i'(t), y_i'(t), 1). \tag{21}$$

Interpolation methods or finite differences (forward, backward or central) approximation can be used with sampled data.

4 Methodology

This section is organized in three parts. The first part presents the derivation of the spatio-temporal discretization framework using a data-driven approach. In the second part, we define pedestrian traffic variables, that is density, flow and velocity. The variables are defined by revising the existing microscopic definitions according to the proposed discretization (as motivated in Section 2). In the third part, we present concrete suggestions for the operationalization of the general and abstract concepts related to the discretization framework.

4.1 Data-driven discretization

We propose the discretization in space and time that is defined based on three-dimensional (3D) Voronoi diagrams associated with pedestrian trajectories. We call the set of trajectories the generator set $\Gamma = \{\Gamma_1, ..., \Gamma_n\}$, consistently with the literature. We assume that elements in Γ do not intersect each other. This assumption is reasonable, as two pedestrians cannot be at the exact same place at the exact same time. The main idea for defining the partition of Ω is that (i) every point $p \in \Omega$ belongs to a unique discretization unit, (ii) each discretization unit is assigned to one generator $\Gamma_i \in \Gamma$ according to a certain assignment rule and (iii) the resulting discretization units associated with the trajectories are collectively exhaustive and mutually exclusive. Therefore, the partitioning is characterized by the assignment of each point $p \in \Omega$ to one generator from Γ. The discretization units are then defined as the set of points p assigned to the same generator.

Given a non-empty space Ω and a generator set Γ, the assignment rule δ_Γ of a point $p \in \Omega$ to an element of Γ is in the literature (Okabe et al., 2000) often

specified in terms of distance relations D (not necessary distance metric). The point p is assigned to the "closest" generator in term of a given distance:

$$\delta_\Gamma(p, \Gamma_i) = \begin{cases} 1, & D(p, \Gamma_i) \leq D(p, \Gamma_j), \forall j \neq i \\ 0, & \text{otherwise.} \end{cases} \tag{22}$$

Note that this rule is ambiguous for points p that are equidistant to two trajectories. In this case, an additional arbitrary rule must be used. For instance, if $D(p, \Gamma_i) = D(p, \Gamma_j)$, then it can be decided that p is assigned to Γ_i if $i \leq j$.

If the generators are continuous trajectories (19), the distance may be defined as

$$D(p, \Gamma_i) = \min_t \{d(p, p_i(t)) | p_i(t) \in \Gamma_i, \Gamma_i \in \Gamma, p \in \Omega\}, \tag{23}$$

where $d(p, q)$ is the distance between two points p and q in Ω. Concrete examples of this distance function are discussed in Section 4.3. Similarly, if the generators are sampled (20), the distance may be defined as

$$D(p, \Gamma_i) = \min_s \{d(p, p_{is}) | p_{is} \in \Gamma_i, \Gamma_i \in \Gamma, p \in \Omega\}. \tag{24}$$

Under the assignment rule (22), we consider the set of points V_i assigned to Γ_i

$$V_i = \{p | \delta_\Gamma(p, \Gamma_i) = 1, p \in \Omega, \Gamma_i \in \Gamma\}, \tag{25}$$

which represents a personal spatio-temporal region associated with pedestrian i. For each i, V_i is a convex subset of Ω called a Voronoi cell. Collectively, they represent a Voronoi diagram. The assumption that Ω is obstacle-free and bounded (Section 3) allows for the creation of non-degenerate Voronoi diagrams

$$\mathcal{V} = \{V_1, ..., V_n\}, \tag{26}$$

generated by Γ.

In a three-dimensional space Ω the plane through the point $p_0 = (x_0, y_0, t_0)$ and with non-zero normal vector $\vec{n} = (a, b, c)$ has equation

$$\mathcal{P}_{\vec{n}, p_0} : ax + by + ct + d = 0, \tag{27}$$

where $d = -ax_0 - by_0 - ct_0$. We define the set of points $A(V_i, \mathcal{P}_{\vec{n}, p_0})$ corresponding to the intersection of the cell V_i and the plane $\mathcal{P}_{\vec{n}, p_0}$

$$A(V_i, \mathcal{P}_{\vec{n}, p_0}) = \{p | p \in \{V_i \cap \mathcal{P}_{\vec{n}, p_0}\}\}. \tag{28}$$

For $\vec{n} = (0, 0, 1)$ we have a plane parallel to the x-y plane and its intersection with V_i is given as

$$A(V_i, \mathcal{P}_{(0,0,1), p_0}) = \{p | p \in V_i \text{ and } p_t = t_0\}. \tag{29}$$

It represents a set of dimension 2 or a physical area on the floor (illustrated in Figure 1(a)), at time t_0. The area of this cell is denoted by $|A(V_i, \mathcal{P}_{(0,0,1),p_0})|$, with the unit in m^2. Similarly, for $\vec{n} = (a, b, 0)$ we have

$$A(V_i, \mathcal{P}_{(a,b,0),p_0}) = \{p | p \in V_i \text{ and } ap_x + bp_y = ax_0 + by_0\}. \tag{30}$$

It is the set of dimension 2 or a segment on the floor occupied by pedestrian i in the direction perpendicular to $\vec{n} = (a, b, 0)$ during the time interval spanning V_i. The area of the cell is denoted by $|A(V_i, \mathcal{P}_{(a,b,0),p_0})|$, with the unit in ms. Note that if $\vec{n} = (1, 0, 0)$ and $\vec{n} = (0, 1, 0)$, the corresponding planes are parallel to the x-t, respectively the y-t plane (illustrated in Figure 1(b)).

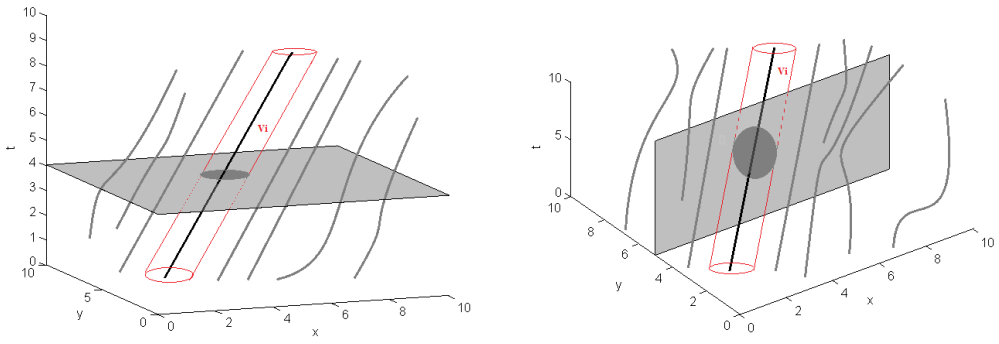

(a) Set in V_i for a specific time t (b) Set in V_i for a specific location y

Figure 1: 3D Voronoi-based discretization

4.2 Definitions of pedestrian traffic variables

Assume that the Voronoi cell V_i is associated with position $(x, y, t) \in \Omega$. The density at (x, y, t) is defined as the inverse of the area of the set $A(V_i, \mathcal{P}_{(0,0,1),(x,y,t)})$ assigned to pedestrian i at time t

$$k(x, y, t) = \frac{1}{|A(V_i, \mathcal{P}_{(0,0,1),(x,y,t)})|}, \tag{31}$$

where $A(V_i, \mathcal{P}_{(0,0,1),(x,y,t)})$ is given by (29) and $|A(V_i, \mathcal{P}_{(0,0,1),(x,y,t)})|$ is the area of this set. The location (x, y) determines pedestrian i and the corresponding set $A(V_i, \mathcal{P}_{(0,0,1),(x,y,t)})$. The unit of $k(x, y, t)$ is a number of pedestrians per square meter. This definition is consistent with (11), adapted to this 3D Voronoi context.

The flow in the direction determined by the vector $\vec{e} = (a, b)$ is defined as the inverse of the area of the set $A(V_i, \mathcal{P}_{(a,b,0),(x,y,t)})$ assigned to pedestrian i

$$\vec{q}_e(x, y, t) = \frac{1}{|A(V_i, \mathcal{P}_{(a,b,0),(x,y,t)})|}, \tag{32}$$

where $A(V_i, \mathcal{P}_{(a,b,0),(x,y,t)})$ is given by (30) and $|A(V_i, \mathcal{P}_{(a,b,0),(x,y,t)})|$ is the area of this set. The point (x, y, t) determines pedestrian i and the corresponding set $A(V_i, \mathcal{P}_{(a,b,0),(x,y,t)})$. The set $(V_i, \mathcal{P}_{(a,b,0),(x,y,t)})$ belongs to the spatio-temporal domain. Therefore, the unit of $\vec{q}_e(x, y, t)$ is a number of pedestrians per meter per second. The flow in x and y directions is obtained considering the inverse of the areas $|A(V_i, \mathcal{P}_{(1,0,0),(x,y,t)})|$ and $|A(V_i, \mathcal{P}_{(0,1,0),(x,y,t)})|$, consistently with (12).

Adopting the usual definition of the velocity (the ratio between the flow and density), from (31) and (32) we have

$$\vec{v}_e(x, y, t) = \frac{\vec{q}_e(x, y, t)}{k(x, y, t)} = \frac{|A(V_i, \mathcal{P}_{(0,0,1),(x,y,t)})|}{|A(V_i, \mathcal{P}_{(a,b,0),(x,y,t)})|}. \tag{33}$$

It represents the mean speed of pedestrian i (Jabari et al., 2014) in the direction determined by the vector $\vec{e} = (a, b)$, expressed in meters per second.

Note that the framework allows for the specification and measurement of the indicators $\vec{q}_e(x, y, t)$ and $\vec{v}_e(x, y, t)$ in any direction $\vec{e}$ of interest. Our approach is microscopic and therefore suitable for multi-directionl nature of pedestrian flows. As discussed in Section 2, the macroscopic approach is often used in the literature, which may not always result in the desired outcome. Consider the case where half of pedestrians walk in one direction and the rest in the opposite direction, and both with the same speed. Their velocity and flow vectors would cancel out at the aggregate level, but the issue does not appear at the microscopic level. Also, the proposed definitions are able to preserve the heterogeneity of pedestrians, due to their microscopic nature.

We refer to the proposed approach as the *3D Voronoi characterization* (3DVoro).

4.3 Spatio-temporal distances

The proposed framework is fairly general, and can accommodate various methods to generate the Voronoi diagrams, based on different definitions of the distance between two points. To construct 3D Voronoi diagrams (Section 4.1), we need to define the exact form of the distance relation d used in (23) and (24). Applying the Euclidean distance in $\mathbb{R}^3$ looks like a natural choice. However, it is important to keep in mind that it would mix units in square meters with units in seconds. We propose here several ways to deal with it. First, we propose to restrict the

Euclidean distance in the spatial dimension, and consider each point in time as independent. Second, we propose distances in $\mathbb{R}^3$ that convert seconds into meters using speed. Third, we account for the pedestrian dynamics to define the distance, anticipating his future position. Finally, we define a distance through the identification of points that are equidistant. Their respective performance is empirically evaluated in Section 5.

We denote by $p = (x, y, t)$ a point from Ω. An observation from the trajectory of pedestrian i is denoted by $p_i = (x_i, y_i, t_i)$. It refers to either $p_i(t)$ or p_{is}, depending on the context.

4.3.1 Spatial Euclidean distance

The first distance that we propose is defined with respect to the standard Euclidean distance in the spatial dimension, that is

$$d_E(p, p_i) = \begin{cases} \sqrt{(x - x_i)^2 + (y - y_i)^2}, & t = t_i \\ \infty, & \text{otherwise.} \end{cases} \tag{34}$$

Intuitively, each point in time is independent. This is motivated by the availability of snapshots of the floor area at given points in time. This implies that all pedestrians in the area must be observed at the exact same time. In practice, it means that the use of this distance is applicable only on continuous trajectories. When sampled trajectories are available (see discussion in Section 3), interpolation should be used to generate the continuous ones.

We refer to the characterization obtained using this distance as the *Euclidean 3D Voronoi characterization* (E-3DVoro).

4.3.2 Time-Transform distances

We define the set of three distances that apply a conversion parameter, expressed in meters per second, to transform the temporal difference between the points into the spatial one. They are denoted as the Time-Transform distances (d_{TT_1}, d_{TT_2}, d_{TT_3}). The distances differ in terms of the choice of the conversion parameter and in the way of coupling the spatial and temporal component. They are defined as

$$d_{TT_1}(p, p_i) = \sqrt{(x - x_i)^2 + (y - y_i)^2 + v^2(t - t_i)^2}, \tag{35}$$

where v is a parameter representing the typical speed of pedestrians (a value of v = 1.34 m/s is used in our experiments, Weidmann (1993)),

$$d_{TT_2}(p, p_i) = \sqrt{(x - x_i)^2 + (y - y_i)^2 + \hat{v}_i(t_i)^2(t - t_i)^2}, \text{ and} \tag{36}$$

$$d_{TT_3}(p, p_i) = \sqrt{(x - x_i)^2 + (y - y_i)^2} + \hat{v}_i(t_i)|t - t_i|, \tag{37}$$

where $\hat{v}_i(t_i)$ is the speed at time t on trajectory Γ_i. The choice of the conversion parameter $\hat{v}_i(t_i)$ in (36) and (37) allows to treat moving pedestrians in a different way than standing pedestrians.

The distances (35) and (36) combine the spatial and temporal components based on the Euclidean norm, using two different values for the speed. In (37), the components are considered as independent and kept separately. The distance d_{TT_3} is defined as a weighted sum of two norms. When $t = t_i$, all distances are equivalent to (34).

We refer to the characterization obtained using these three distances as the *Time-Transform 3D Voronoi characterization* (TT_1-3DVoro, TT_2-3DVoro and TT_3-3DVoro).

4.3.3 Predictive distance

The Predictive distance anticipates the forward movement of pedestrians. The anticipated positions x_i^a and y_i^a are extrapolated from the current velocities of pedestrians for a time determined by the anticipation time $t - t_i$

$$x_i^a = x_i^a(t) = x_i + (t - t_i)v_i^x(t_i), \tag{38}$$

$$y_i^a = y_i^a(t) = y_i + (t - t_i)v_i^y(t_i), \tag{39}$$

where $v_i^x(t_i)$ and $v_i^y(t_i)$ are the speed of pedestrian i at t_i in x, respectively y, direction.

The distance is specified as

$$d_P(p, p_i) = \begin{cases} \sqrt{(x_i^a - x)^2 + (y_i^a - y)^2}, & t - t_i \geq 0 \\ \infty, & \text{otherwise.} \end{cases} \tag{40}$$

Note that it is not a metric distance, as it is not symmetric. The anticipation time extends from zero to a positive value $(t - t_i)$. Points p that are backward in time with respect to the current positions of pedestrian are considered infinitely distant. When $t = t_i$, the distance reduces to the standard $\mathbb{R}^2$ Euclidean distance. The consideration of individual speeds allows for the distinction between pedestrians that perform movement from those that stand.

We refer to the characterization obtained using this distance as the *Predictive 3D Voronoi characterization* (P-3DVoro).

4.3.4 Mahalanobis distance

The Mahalanobis distance is specified as

$$d_M(p, p_i) = \sqrt{(p - p_i)^T M_i (p - p_i)}, \tag{41}$$

where M_i is a change of variable matrix. It is a symmetric, positive-definite matrix, which defines how the distances are measured in different spatio-temporal directions from the perspective of pedestrian i. To implement this distance we need to determine the matrix M_i. We do so by identifying 6 points in Ω such that they are equidistant to p_i for the Mahalanobis distance. We take into account the information about the speed and direction of pedestrians, in the sense that the points that are in the movement direction of a pedestrian are "closer" than the points from other directions.

Formally, we consider three directions of interest. First, we define the normalized direction of movement in the space-time dimensions

$$d^1(t_i) = \frac{v_i(t_i)}{\|v_i(t_i)\|}, \|d^1(t_i)\| = 1, \tag{42}$$

where $v_i(t_i)$ is the speed along the trajectory of pedestrian i given by (21). We next define a normalized spatial direction orthogonal to $d^1(t_i)$, that is

$$d^2(t_i) = \begin{pmatrix} d^1_x(t_i) \\ d^2_y(t_i) \\ 0 \end{pmatrix}, \tag{43}$$

such that $d^1(t_i)^T d^2(t_i) = 0$ and $\|d^2(t_i)\| = 1$. The third direction is for time

$$d^3(t_i) = \begin{pmatrix} 0 \\ 0 \\ \Delta t \end{pmatrix}, \tag{44}$$

where Δt is typically determined by the sampling frequency and $\|d^3(t_i)\| = \Delta t$.

We determine the matrix M_i, and the distance d_M, such that the following points in the defined directions are all at distance α from the point p_i. The key feature is that, in the direction of movement, the distances do not refer to the position at time t, but the positions at time $t + \Delta t$ and $t - \Delta t$. The points S_1 and S_2 in the d^1 direction are at α and $-\alpha$ from the positions at time $t + \Delta t$, respectively $t - \Delta t$

$$S_1(t_i, \alpha) = p_i + \Delta t v_i(t_i) + \alpha d^1(t_i), \tag{45}$$

$$S_2(t_i, \alpha) = p_i - \Delta t v_i(t_i) - \alpha d^1(t_i). \tag{46}$$

In the direction d^2 we consider the point S_3 that is at α from the point p_i

$$S_3(t_i, \alpha) = p_i + \alpha d^2(t_i), \tag{47}$$

and the point S_4 that is at $-\alpha$ from the point p_i

$$S_4(t_i, \alpha) = p_i - \alpha d^2(t_i). \tag{48}$$

Similarly, in time direction d^3 we consider the point S_5 that is at α from the point p_i

$$S_5(t_i, \alpha) = p_i + \alpha d^3(t_i), \tag{49}$$

and the point S_6 that is at $-\alpha$ from the point p_i

$$S_6(t_i, \alpha) = p_i - \alpha d^3(t_i). \tag{50}$$

This is illustrated in Figure 2.

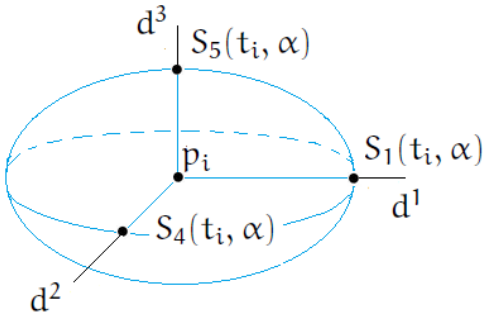

Figure 2: Mahalanobis distance - illustration

In standard Euclidean space we have that

$$||S_1(t_i, \alpha) - p_i|| = ||S_2(t_i, \alpha) - p_i|| = \Delta t||v_i(t_i)|| + \alpha. \tag{51}$$

It shows that, in the direction d^1, the forward and backward distances are stretched by the quantity $\Delta t||v_i(t_i)||$. This is designed to anticipate the movement of pedestrians. The additional term vanishes when $\Delta t \to 0$. The approach also allows to deal with moving pedestrians and standing pedestrians in a different way. The distance in the d^2 direction is consistent with Euclidean distance

$$||S_3(t_i, \alpha) - p_i|| = ||S_4(t_i, \alpha) - p_i|| = ||\alpha d^2(t_i)|| = \alpha. \tag{52}$$

The distance in time direction d^3 is proportional to the time discretization

$$||S_5(t_i, \alpha) - p_i|| = ||S_6(t_i, \alpha) - p_i|| = ||\alpha d^3(t_i)|| = \alpha \Delta t. \tag{53}$$

In particular, it shrinks to zero when $\Delta t \to 0$.

In our experiments, a value of $\alpha = 1$ is used.

We refer to the characterization obtained using this distance as the *Mahalanobis 3D Voronoi characterization* (M-3DVoro).

5 Empirical analysis

The performance of our approach is evaluated using synthetic data. Pedestrian trajectories are synthesized using the NOMAD simulation tool (Campanella, 2010) for uni-directional flow composition. The flow is simulated in a 4 meters by 4 meters area, as illustrated in Figure 3, during 10 seconds. Pedestrians originate from the white rectangle on the left, and finish their trips at the destination represented by the gray rectangle. The direction of the flow is denoted by the arrow.

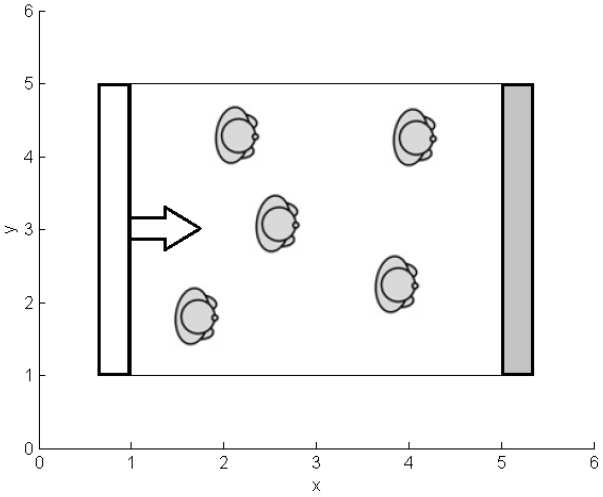

Figure 3: Uni-directional flow simulation: the bounding-box of the simulation area

The analysis is done for two different scenarios. In the first scenario, we consider low congestion and homogeneous pedestrian population ($S_{\mathrm{LC-HomoPop}}$). Low congestion regime is simulated assuming a uniform demand of 1.2 pedestrians per second over the period of simulation. The homogeneity of the population is reflected through (approximately) homogenous walking speed of pedestrians. We use the average speed value of 1.34 m/s, according to the study of Weidmann (1993). In the second scenario, we consider high congestion and heterogeneous pedestrian population ($S_{\mathrm{HC-HeteroPop}}$). The demand of 3.6 pedestrians per second is considered to produce higher congestion. To represent the heterogeneity in the population, we consider three sub-populations (slow, average and fast) with respective speeds of 0.5 m/s, 1.3 m/s and 2.1 m/s. Each sub-population has roughly the same size.

Our objective is to analyze the robustness of the approach with respect to the simulation noise and with respect to the sampling frequency. 3DVoro (for all the distances) is compared with the approaches proposed in the literature on both

scenarios $S_{LC-HomoPop}$ and $S_{HC-HeteroPop}$. Duives et al. (2015) have performed empirical comparisons of the existing approaches and concluded that the XY-T and VB methods (Section 2.2) perform the best. For this reason our approach will be compared only with these two methods. In the application of the XY-T method, the parameters reported in Duives et al. (2015) are used: a time interval of 1 second, and a grid cell size of 1×1 meter. Note that, the VB method corresponds to the E-3DVoro when used for the discrete time instants to discretize the spatial dimension only. Therefore, the VB method will not be considered separately.

5.1 Pedestrian flow characterization based on trajectories

In this section we analyze the performance of the approach when pedestrian trajectory data is available in the form of an analytical description. We synthesize 100 sets of pedestrian trajectories for each scenario and evaluate the variance of the indicators across these replications. The described settings of the simulator remain unchanged for a given scenario. The indicators (k, v, q) are calculated for each set of the trajectories via 3DVoro (for all the distances) and the XY-T method. The methods are compared based on the standard deviation of the indicators at specific points due to simulation noise.

Let M represent the method (3DVoro or XY-T), r a realization of NOMAD simulation ($r = 1, ..., 100$) and p a point from Ω. We denote by $\theta_r^M(p) = (k_r^M(p), v_r^M(p), q_r^M(p))$ a vector of indicators at point p obtained by applying the method M to the r^{th} set of trajectories. For each method we calculate the standard deviation of the indicators at p as

$$\sigma_R^M(p) = \sqrt{\frac{1}{R}\sum_{r=1}^{R}(\theta_r^M(p) - \mu_R^M(p))^2}, \tag{54}$$

where $\mu_R^M(p) = \frac{1}{R}\sum_{r=1}^{R}\theta_r^M(p)$ and $R = 100$. This procedure is repeated for 1000 randomly selected points p (these points are the same across simulation). The results are reported using boxplot representation in Figure 4 for $S_{LC-HomoPop}$, and in Figure 5 for $S_{HC-HeteroPop}$.

The standard deviations of the indicators are larger for $S_{HC-HeteroPop}$ for all the methods, compared to $S_{LC-HomoPop}$. This can be explained by the larger changes in the data due to higher complexity of the system in $S_{HC-HeteroPop}$. However, a similar trend is noticeable in the results for both scenarios.

The results suggest that the changes of trajectories, even though for the same simulated settings, dramatically affect the measured indicators of the XY-T method. Larger values of the standard deviation occur in this case due to the fact that entering or exiting of the discretization unit by a person affects the indicators considerably.

Compared to the XY-T method, the 3DVoro provides lower standard deviations. The results for the density indicator (Figure 4 (a) and Figure 5 (a)), and for the flow indicator (Figure 4 (b) and Figure 5 (b)), are similar across different 3DVoro distances for both scenarios. In the case of speed, E-3DVoro exhibits larger standard deviations as compared to other 3DVoro methods for $S_{\mathrm{LC-HomoPop}}$ (Figure 4 (c)). This suggests that 3DVoro with distances that account for the speed and/or movement direction of pedestrians lead to lower variance in the results when congestion is low. When congestion is higher (Figure 5 (c)), higher number of pedestrian trajectories leads to similar behavior of different distances, and consequently to similar results.

5.2 Pedestrian flow characterization based on sampled data

In order to evaluate the effectiveness of the approach when sampled data is available, we consider the samples of points from the synthetic trajectories. The samples are obtained using different sampling frequencies: 3 s^{-1}, 2 s^{-1}, 1 s^{-1} and 0.5 s^{-1}. The feature of interest is the robustness of the approach with respect to the sampling frequency. That is, the ability of the approach to produce stable results even in the lack of continuous observations.

We can deal with sampled data in two ways. First, we generate continuous trajectories using linear interpolation. Note that, simple linear interpolation generates non differentiable trajectories. The speed along trajectories is approximated, using finite differences. The indicators are then obtained via 3DVoro applied to the interpolated trajectories. In the second case we apply 3DVoro directly to the sampled data. The indicators calculated on the true synthetic trajectories are used as a benchmark. The indicators obtained using samples and interpolated trajectories are compared at 1000 randomly selected points to the corresponding benchmark values. These points are the same across all the methods.

We list in Table 2 and Table 3 the statistics (mean, mode, median and 90%-quantile) corresponding to resulting differences in the case of density indicator, for $S_{\mathrm{LC-HomoPop}}$, respectively $S_{\mathrm{HC-HeteroPop}}$. The statistics show similar trends for velocity and flow indicators, as illustrated in Appendix A (Table 4 - Table 7). To demonstrate the performance, we show the results corresponding to the extreme values of the considered sampling frequencies (3 s^{-1} and 0.5 s^{-1}). In the tables, IT refers to the value of a given statistic obtained based on interpolated trajectories; SoP refers to the value of a given statistic obtained based on sample of points. Lighter gray color of the cells in the tables is used to indicate better value between the two (IT and SoP). Darker gray cell color indicates the overall best value of the considered statistic. Note that, E-3DVoro and the XY-T method can be applied only with the trajectories described analytically. Their performance is therefore evaluated only when the points from samples are interpolated.

In general, the 3DVoro method outperforms the XY-T method. The lowest differences between the indicators calculated based on sample of points or interpolated trajectories and the benchmark vales are achieved using the 3DVoro method (Table 2 and Table 3).

The interpolation appears to be a better choice for 3DVoro when the sampling frequency is high, in both scenarios. This is expected, given that more data points used for interpolation yield lower interpolation error. In this case, the Time-Transform distances lead to the best performance of the 3DVoro approach, and in particular TT_1-3DVoro.

When the sampling frequency is low, 3DVoro applied directly to the sample is associated with the best effectiveness. In $S_{LC-HomoPop}$, the distances that are designed to anticipate the movement of pedestrians (P-3DVoro and M-3DVoro) are the most satisfactory. In $S_{HC-HeteroPop}$, the preferred characterization is based on the Time-Transform distances (particularly TT_1-3DVoro).

In summary, the analysis of the indicators suggests that (i) when more data is available, either because of higher sampling frequency or higher congestion (higher number of people), the *Time-Transform 3D Voronoi characterization* (TT_1-3DVoro) is the most robust with respect to the sampling frequency; (ii) when less data is available, due to lower sampling frequency and lighter traffic conditions (lower number of people), the anticipating distances (P-3DVoro and M-3DVoro) exhibit the best robustness.

Method	Mean		Mode		Median		90% quantile	
	IT	SoP	IT	SoP	IT	SoP	IT	SoP
XY-T	1.47E-02	/	1.25E-02	/	1.25E-02	/	6.25E-02	/
E-3DVoro	1.17E-02	/	0	/	4.48E-04	/	3.96E-02	/
TT_1-3DVoro	2.70E-03	6.70E-03	0	0	3.00E-04	2.30E-03	7.30E-03	1.02E-02
TT_2-3DVoro	5.80E-03	3.50E-02	0	2.80E-03	6.00E-04	2.08E-02	1.50E-02	6.69E-02
TT_3-3DVoro	5.40E-03	4.34E-02	0	8.00E-03	6.00E-04	2.83E-02	1.32E-02	9.22E-02
P-3DVoro	8.20E-03	5.36E-02	0	6.10E-03	2.40E-03	3.03E-02	1.30E-02	1.14E-01
M-3DVoro	4.50E-03	5.65E-02	0	6.80E-03	1.10E-03	4.55E-02	1.28E-02	1.04E-01

(a) Sampling frequency: 3 s^{-1}

Method	Mean		Mode		Median		90% quantile	
	IT	SoP	IT	SoP	IT	SoP	IT	SoP
XY-T	1.90E-01	/	1.00E-01	/	1.50E-01	/	3.38E-01	/
E-3DVoro	1.64E-01	/	1.12E-02	/	1.46E-01	/	3.02E-01	/
TT_1-3DVoro	2.54E-01	1.27E-01	1.35E-02	9.00E-03	1.16E-01	8.97E-02	3.41E-01	2.25E-01
TT_2-3DVoro	1.64E-01	1.22E-01	1.44E-02	1.06E-02	1.21E-01	7.30E-02	3.52E-01	2.33E-01
TT_3-3DVoro	1.89E-01	1.24E-01	1.84E-02	1.09E-02	1.24E-01	7.88E-02	3.40E-01	2.31E-01
P-3DVoro	3.19E-01	1.21E-01	3.26E-02	6.20E-03	1.43E-01	7.43E-02	3.36E-01	2.10E-01
M-3DVoro	1.97E-01	1.24E-01	3.48E-02	9.90E-03	1.41E-01	7.72E-02	3.21E-01	2.31E-01

(b) Sampling frequency: 0.5 s^{-1}

Table 2: Robustness to the sampling frequency of density indicator - $S_{LC-HomoPop}$

Method	Mean		Mode		Median		90% quantile	
	IT	SoP	IT	SoP	IT	SoP	IT	SoP
XY-T	2.05E-02	/	0	/	1.25E-02	/	5.00E-02	/
E-3DVoro	1.43E-02	/	0	/	2.67E-02	/	2.64E-02	/
TT_1-3DVoro	8.00E-03	4.55E-02	0	0	8.00E-04	1.75E-02	2.36E-02	8.52E-02
TT_2-3DVoro	1.49E-02	1.07E-01	0	0	3.20E-03	5.72E-02	3.33E-02	2.21E-01
TT_3-3DVoro	1.24E-02	1.60E-01	0	0	3.50E-03	9.62E-02	2.98E-02	3.41E-01
P-3DVoro	2.10E-02	1.66E-01	0	0	4.20E-03	1.16E-01	5.27E-02	3.64E-01
M-3DVoro	1.31E-02	2.40E-01	0	0	2.50E-03	1.75E-01	2.91E-02	5.58E-01

(a) Sampling frequency: 3 s^{-1}

Method	Mean		Mode		Median		90% quantile	
	IT	SoP	IT	SoP	IT	SoP	IT	SoP
XY-T	5.29E-01	/	1.63E-01	/	4.75E-01	/	1.01E00	/
E-3DVoro	4.02E-01	/	0	/	2.49E-01	/	1.03E+00	/
TT_1-3DVoro	4.06E-01	2.90E-01	3.10E-01	2.48E-02	2.64E-01	1.65E-01	9.21E-01	7.12E-01
TT_2-3DVoro	3.92E-01	4.58E-01	2.85E-01	2.34E-01	2.48E-01	2.34E-01	9.30E-01	1.11E+00
TT_2-3DVoro	4.41E-01	5.07E-01	2.89E-01	5.89E-02	2.37E-01	3.06E-01	9.81E-01	1.17E+00
P-3DVoro	4.31E-01	3.71E-01	1.40E-03	0	2.58E-01	1.80E-01	9.43E-01	7.29E-01
M-3DVoro	4.34E-01	5.01E-01	3.16E-01	1.36E-01	2.75E-01	3.52E-01	9.96E-01	9.80E-01

(b) Sampling frequency: 0.5 s^{-1}

Table 3: Robustness to the sampling frequency of density indicator - $S_{\mathrm{HC-HeteroPop}}$

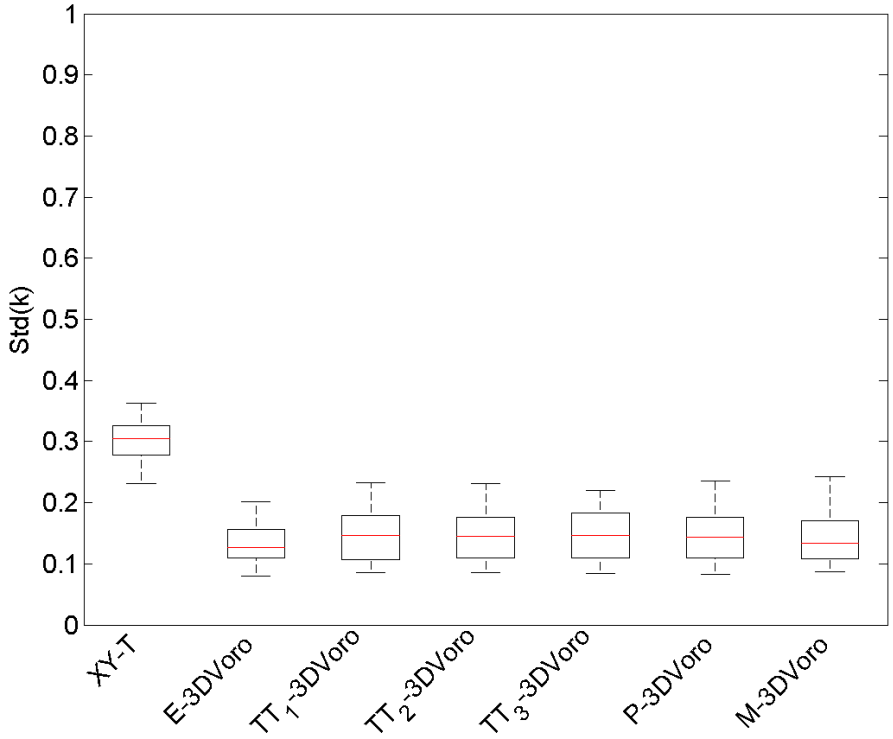

(a) Standard deviation of density indicator

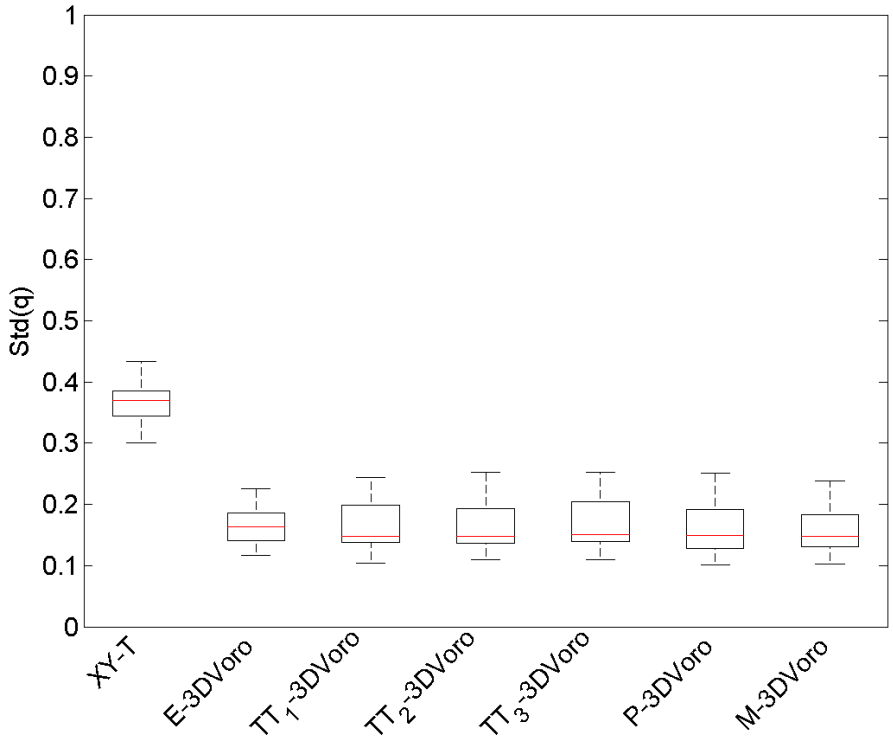

(b) Standard deviation of flow indicator

Figure 4: Robustness to the simulation noise - $S_{\mathrm{LC-HomoPop}}$

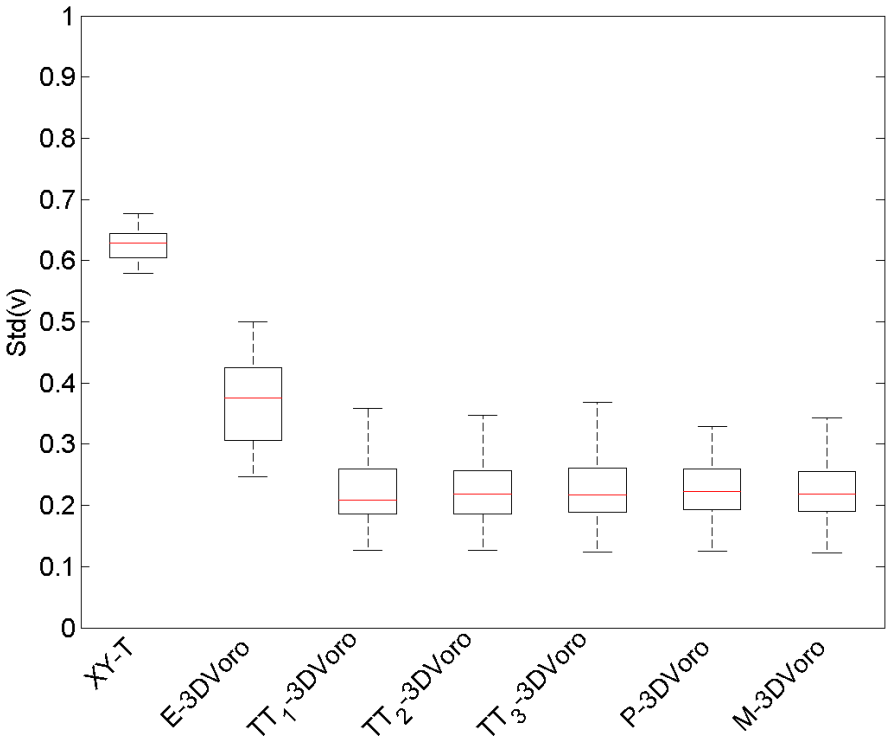

(c) Standard deviation of velocity indicator

Figure 4: Robustness to the simulation noise - $S_{LC-HomoPop}$ (cont.)

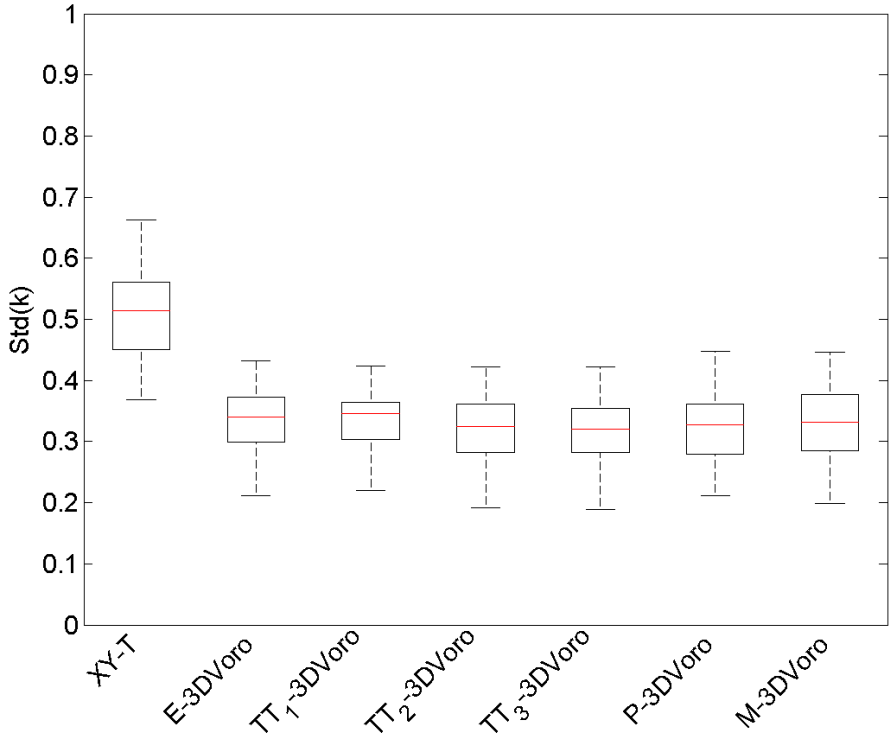

(a) Standard deviation of density indicator

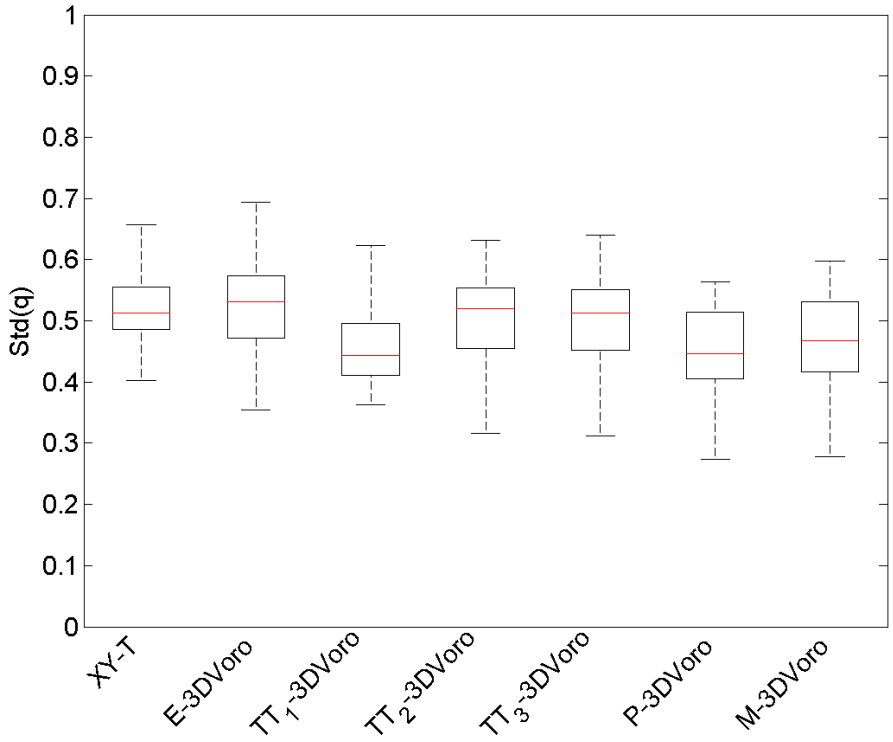

(b) Standard deviation of flow indicator

Figure 5: Robustness to the simulation noise - $S_{\mathrm{HC-HeteroPop}}$

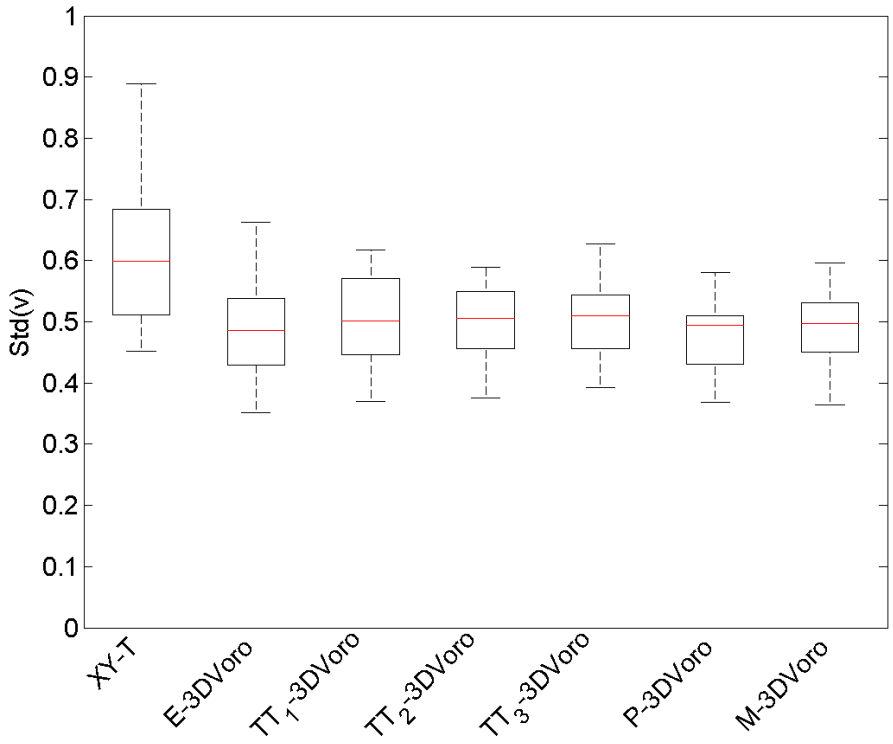

(c) Standard deviation of velocity indicator

Figure 5: Robustness to the simulation noise - $S_{\mathrm{HC-HeteroPop}}$ (cont.)

6 Conclusion

In this paper a novel methodology for pedestrian traffic characterization is proposed. The definitions of pedestrian traffic variables that we have put forward are based on data-driven partitioning in space and time, avoiding the need to define an arbitrary discretization. The disretization framework is designed via three-dimensional Voronoi diagrams directly generated from pedestrian trajectory data. It can be designed based on trajectories available either in the form of an analytical description or as a finite collection of points. The methodological framework is fairly general, and the exact characterization of the Voronoi diagrams can be adapted to specific situations. We have proposed different definitions of distances for the construction of the diagrams, and assessed them in quantitative terms. Also, the proposed definitions of the indicators are microscopic. They are therefore able to reflect the heterogeneity of pedestrians, and suitable for the multi-directional composition of pedestrian flows.

The performance of the proposed approach is evaluated using synthetic data generated for two different uni-directional scenarios. It has been shown, for these data sets, that our approach outperforms the considered approaches from the literature, in terms of the variance of the results and the robustness with respect to the sampling frequency. For continuous trajectories, 3DVoro with distances that account for the speed and/or movement direction of pedestrians lead to lower variance in the results when congestion is low. When congestion is higher, higher number of data leads to similar behavior of different distances, and consequently to similar results. For sampled data, when the sampling frequency is high, 3DVoro based on interpolated trajectories shows better results. When the sampling frequency is low, 3DVoro based on sample of points exhibit better performance. The analysis in the case of sampled data suggests that the *Time-Transform 3D Voronoi characterization* is the most robust with respect to the sampling frequency when more data is available. When less data is available, the anticipating distances lead to the best robustness with respect to the sampling.

More research is needed to determine the performance of the approach in other behavioral situations and to understand its potential limitations. For instance, we have started to evaluate the approach for bi-directional and multi-directional scenarios, in light of different speed and congestion regimes. Additionally, we will examine the effectiveness of the approach using real data (described in Nikolić et al. (2016)). A sensitivity analysis for the conversion parameter ν in TT_1-3DVoro, and the α parameter in M-3DVoro is another direction of the investigation.

The set of distances proposed in this paper to characterize the Voronoi diagrams can be extended. In particular, an interesting research topic would be to relate the definition of the distance with some behavioral assumptions about the pedestrian movements. For example, it has been recognized that pedestrians are

affected much stronger by stimuli that appear within their vision field (Johansson et al., 2007). To account for the anisotropy of pedestrian movements, weighted versions of the proposed distances could be further studied. The weights would be modeled based on the movement direction of pedestrians and their vision field.

Our future research will also be directed towards the characterization in the presence of obstacles. One possibility would be to extend a generator set from pedestrian trajectories to trajectories and areas, where areas represent obstacles. This would result in three-dimensional discretization where each pedestrian and each obstacle are associated with their own, non-overlaping, spatio-temporal units.

A Appendix

Method	Mean		Mode		Median		90% quantile	
	IT	SoP	IT	SoP	IT	SoP	IT	SoP
XY-T	4.30E-03	/	0	/	3.40E-03	/	1.16E-02	/
E-3DVoro	1.55E-01	/	0	/	3.56E-02	/	4.99E-01	/
TT_1-3DVoro	9.60E-03	2.31E-02	0	0	2.20E-03	9.38E-03	2.79E-02	4.85E-02
TT_2-3DVoro	2.04E-02	7.66E-02	0	4.10E-03	5.80E-03	4.48E-02	6.48E-02	1.68E-01
TT_3-3DVoro	1.81E-02	9.15E-02	0	8.00E-04	5.70E-03	4.51E-02	5.42E-02	2.15E-01
P-3DVoro	2.98E-02	1.38E-01	0	5.90E-03	1.41E-02	7.90E-02	5.75E-02	2.92E-01
M-3DVoro	1.88E-02	1.46E-01	0	2.00E-04	5.90E-03	1.04E-01	5.95E-02	3.22E-01

(a) Sampling frequency: 3 s^{-1}

Method	Mean		Mode		Median		90% quantile	
	IT	SoP	IT	SoP	IT	SoP	IT	SoP
XY-T	5.80E-01	/	1.02E+00	/	3.26E-01	/	1.42E+00	/
E-3DVoro	1.77E+00	/	4.36E-02	/	7.11E-01	/	1.27E+00	/
TT_1-3DVoro	5.42E-01	5.40E-01	2.28E-02	2.10E-03	3.43E-01	3.02E-01	1.04E+00	9.66E-01
TT_2-3DVoro	5.11E-01	5.56E-01	1.39E-01	8.20E-03	3.15E-01	3.17E-01	1.07E+00	1.04E+00
TT_3-3DVoro	6.08E-01	5.52E-01	3.72E-02	7.50E-03	3.29E-01	3.18E-01	1.05E+00	1.05E+00
P-3DVoro	5.60E-01	5.41E-01	8.75E-02	1.30E-03	3.32E-01	3.04E-01	9.76E-01	9.82E-01
M-3DVoro	5.03E-01	5.43E-01	3.93E-02	6.91E-02	3.76E-01	3.15E-01	1.08E+00	9.52E-01

(b) Sampling frequency: 0.5 s^{-1}

Table 4: Robustness to the sampling frequency of velocity indicator - $S_{LC-HomoPop}$

It is interesting to notice that the XY-T method results in the most satisfactory estimation of speed only in $S_{LC-HomoPop}$ for high sampling frequency (Table 4 (a)). This can be explained by the simulated homogenous speed conditions that the fixed-grid discretization is able to reflect. When the sampling frequency is lower (Table 4 (b)), or when traffic conditions are more complex (Table 5), the performance of this method deteriorates, in regard to the speed estimation.

Method	Mean		Mode		Median		90% quantile	
	IT	SoP	IT	SoP	IT	SoP	IT	SoP
XY-T	1.92E-02	/	9.60E-03	/	6.20E-03	/	3.42E-02	/
E-3DVoro	3.17E-02	/	0	/	6.30E-03	/	3.86E-02	/
TT_1-3DVoro	1.57E-02	6.18E-02	0	0	6.10E-03	1.87E-02	3.23E-02	1.30E-01
TT_2-3DVoro	1.83E-02	1.38E-01	0	1.73E-02	7.90E-03	4.27E-02	3.82E-02	3.88E-01
TT_3-3DVoro	1.85E-02	1.88E-01	0	1.00E-01	8.00E-03	6.46E-02	4.08E-02	4.87E-01
P-3DVoro	2.93E-02	2.05E-01	0	7.96E-02	9.00E-03	9.82E-02	6.49E-02	5.29E-01
M-3DVoro	2.14E-02	3.16E-01	0	5.10E-03	8.00E-03	1.47E-01	4.37E-02	8.21E-01

(a) Sampling frequency: 3 s^{-1}

Method	Mean		Mode		Median		90% quantile	
	IT	SoP	IT	SoP	IT	SoP	IT	SoP
XY-T	5.73E-01	/	1.15E+00	/	3.51E-01	/	1.58E+00	/
E-3DVoro	1.01E+00	/	8.57E-01	/	3.85E-01	/	1.67E+00	/
TT_1-3DVoro	5.82E-01	5.80E-01	8.69E-01	5.85E-02	4.51E-01	3.13E-01	1.40E+00	1.28E+00
TT_2-3DVoro	5.76E-01	5.67E-01	9.40E-01	1.02E-01	3.75E-01	2.64E-01	1.54E+00	1.16E+00
TT_3-3DVoro	5.79E-01	5.94E-01	8.50E-01	5.73E-02	3.70E-01	2.77E-01	1.46E+00	1.29E+00
P-3DVoro	5.66E-01	5.62E-01	8.92E-01	4.61E-02	3.83E-01	2.95E-01	1.38E+00	1.26E+00
M-3DVoro	6.27E-01	7.11E-01	9.13E-01	1.43E-02	5.05E-01	2.86E-01	1.55E+00	1.49E+00

(b) Sampling frequency: 0.5 s^{-1}

Table 5: Robustness to the sampling frequency of velocity indicator - $S_{HC-HeteroPop}$

Method	Mean		Mode		Median		90% quantile	
	IT	SoP	IT	SoP	IT	SoP	IT	SoP
XY-T	1.93E-02	/	0	/	1.77E-02	/	7.73E-02	/
E-3DVoro	1.65E-02	/	0	/	5.60E-03	/	3.75E-02	/
TT_1-3DVoro	3.00E-04	7.60E-03	0	0	0	2.60E-03	8.00E-04	1.74E-02
TT_2-3DVoro	1.40E-03	4.16E-02	0	0	0	3.17E-02	3.60E-03	8.99E-02
TT_3-3DVoro	1.30E-03	4.65E-02	0	4.32E-02	0	3.48E-02	3.90E-03	1.14E-01
P-3DVoro	2.70E-03	4.69E-02	0	1.41E-02	8.00E-04	2.27E-02	5.50E-03	1.29E-01
M-3DVoro	1.20E-03	5.09E-02	0	4.75E-02	0	3.54E-02	2.50E-03	1.23E-01

(a) Sampling frequency: 3 s^{-1}

Method	Mean		Mode		Median		90% quantile	
	IT	SoP	IT	SoP	IT	SoP	IT	SoP
XY-T	2.55E-01	/	1.45E-01	/	2.45E-01	/	5.06E-01	/
E-3DVoro	4.17E-01	/	6.50E-02	/	1.27E-01	/	3.83E-01	/
3DVoro-δ_{TT_1}	1.74E-01	1.50E-01	1.79E-01	8.00E-04	1.13E-01	8.77E-02	3.21E-01	2.98E-01
TT_1-3DVoro	2.07E-01	1.53E-01	1.92E-01	1.00E-04	1.39E-01	8.52E-02	3.71E-01	3.29E-01
TT_2-3DVoro	2.33E-01	1.52E-01	2.05E-01	3.00E-04	1.48E-01	8.46E-02	3.63E-01	3.27E-01
TT_2-3DVoro	2.17E-01	1.43E-01	1.53E-01	1.40E-03	1.34E-01	8.49E-02	3.01E-01	2.98E-01
M-3DVoro	1.75E-01	1.48E-01	1.83E-01	1.00E-04	1.36E-01	9.11E-02	3.43E-01	3.22E-01

(b) Sampling frequency: 0.5 s^{-1}

Table 6: Robustness to the sampling frequency of flow indicator - $S_{LC-HomoPop}$

Method	Mean		Mode		Median		90% quantile	
	IT	SoP	IT	SoP	IT	SoP	IT	SoP
XY-T	2.75E-02	/	2.30E-03	/	1.75E-02	/	7.21E-02	/
E-3DVoro	1.09E-02	/	0	/	8.70E-04	/	2.83E-02	/
TT_1-3DVoro	7.80E-03	6.06E-02	0	0	7.00E-04	1.21E-02	2.22E-02	1.58E-01
TT_2-3DVoro	1.05E-02	1.45E-01	0	0	1.10E-03	6.08E-02	2.78E-02	3.11E-01
TT_3-3DVoro	1.06E-02	2.03E-01	0	0	1.00E-03	8.27E-02	2.19E-02	4.64E-01
P-3DVoro	1.62E-02	1.95E-01	0	4.86E-02	1.80E-03	8.54E-02	3.70E-02	4.90E-01
M-3DVoro	1.29E-02	3.06E-01	0	0	1.60E-03	1.48E-01	2.92E-02	8.95E-01

(a) Sampling frequency: 3 s^{-1}

Method	Mean		Mode		Median		90% quantile	
	IT	SoP	IT	SoP	IT	SoP	IT	SoP
XY-T	5.18E-01	/	3.50E-01	/	4.48E-01	/	1.09E+00	/
E-3DVoro	6.54E-01	/	3.69E-01	/	2.03E-01	/	1.54E+00	/
TT_1-3DVoro	4.99E-01	4.02E-01	1.06E-01	6.49E-02	3.24E-01	1.81E-01	1.35E+00	9.43E-01
TT_2-3DVoro	5.66E-01	4.16E-01	1.47E-01	5.55E-02	2.73E-01	1.73E-01	1.57E+00	1.21E+00
TT_3-3DVoro	5.91E-01	4.45E-01	1.53E-01	1.57E-01	2.94E-01	1.71E-01	1.68E+00	1.31E+00
P-3DVoro	4.81E-01	4.28E-01	5.53E-02	3.98E-02	2.22E-01	1.89E-01	1.34E+00	1.12E+00
M-3DVoro	6.41E-01	4.47E-01	9.07E-02	4.55E-02	3.97E-01	1.73E-01	1.66E+00	1.24E+00

(b) Sampling frequency: 0.5 s^{-1}

Table 7: Robustness to the sampling frequency of flow indicator - $S_{\mathrm{HC-HeteroPop}}$

Acknowledgements

This research is supported by the Swiss National Science Foundation Grant 200021-141099 "Pedestrian dynamics: flows and behavior". We would like to thank Flurin Hänseler, Shadi Sharif Azadeh and Riccardo Scarinci for their invaluable assistance and suggestions.

References

Alahi, A., Bierlaire, M. and Vandergheynst, P. (2014). Robust real-time pedestrians detection in urban environments with a network of low resolution cameras, *Transportation Research Part C: Emerging Technologies* **39**: 113–128.

Bauer, D., Brandle, N., Seer, S., Ray, M. and Kitazawa, K. (2009). Measurement of pedestrian movements: A comparative study on various existing systems, *Pedestrian Behavior: Models, Data Collection and Applications*, Emerald Group Publishing Limited: Bingley, UK.

Beck, C. and Roepstorff, G. (1987). Effects of phase space discretization on the long-time behavior of dynamical systems, *Physica D: Nonlinear Phenomena* **25**(1-3): 173–180.

Çöltekin, A., De Sabbata, S., Willi, C., Vontobel, I., Pfister, S., Kuhn, M. and Lacayo, M. (2011). Modifiable temporal unit problem, *ISPRS/ICA workshop Persistent problems in geographic visualization(ICC2011), Paris, France*, Vol. 2.

Daamen, W. and Hoogendoorn, S. P. (2003). Controlled experiments to derive walking behaviour, *European Journal of Transport and Infrastructure Research* **3**(1): 39–59.

Duives, D. C., Daamen, W. and Hoogendoorn, S. P. (2013). State-of-the-art crowd motion simulation models, *Transportation Research Part C: Emerging Technologies* **37**: 193–209.

Duives, D. C., Daamen, W. and Hoogendoorn, S. P. (2015). Quantification of the level of crowdedness for pedestrian movements, *Physica A: Statistical Mechanics and its Applications* **427**: 162–180.

Edie, L. C. (1963). *Discussion of traffic stream measurements and definitions*, Port of New York Authority.

Fruin, J. J. (1971). Designing for pedestrians: A level-of-service concept, number 355, Highway Research Board, Washington, DC, pp. 1–15.

Hänseler, F., Bierlaire, M., Farooq, B. and Mühlematter, T. (2014). A macroscopic loading model for time-varying pedestrian flows in public walking areas, *Transportation Research Part B: Methodological* **69**: 60 – 80.

Helbing, D., Buzna, L., Johansson, A. and Werner, T. (2005). Self-organized pedestrian crowd dynamics: Experiments, simulations, and design solutions, *Transportation science* **39**(1): 1–24.

Helbing, D., Johansson, A. and Al-Abideen, H. Z. (2007). Dynamics of crowd disasters: An empirical study, *Physical review E* **75**(4): 046109.

Hoogendoorn, S. and Daamen, W. (2004). Self-organization in walker experiments, *Traffic and Granular Flow*, Vol. 3, pp. 121–132.

Hoogendoorn, S. P., van Wageningen-Kessels, F. L., Daamen, W. and Duives, D. C. (2014). Continuum modelling of pedestrian flows: From microscopic principles to self-organised macroscopic phenomena, *Physica A: Statistical Mechanics and its Applications* **416**: 684–694.

Jabari, S. E., Zheng, J. and Liu, H. X. (2014). A probabilistic stationary speed–density relation based on Newell's simplified car-following model, *Transportation Research Part B: Methodological* **68**: 205–223.

Johansson, A., Helbing, D. and Shukla, P. K. (2007). Specification of the social force pedestrian model by evolutionary adjustment to video tracking data, *Advances in complex systems* **10**(supp02): 271–288.

Nikolić, M., Bierlaire, M., Farooq, B. and de Lapparent, M. (2016). Probabilistic speed–density relationship for pedestrian traffic, *Transportation Research Part B: Methodological* **89**: 58–81.

Okabe, A., Boots, B., Sugihara, K. and Chiu, S. N. (2000). *Spatial tessellations: concepts and applications of Voronoi diagrams*, Second edn, Wiley, New York.

Openshaw, S. (1984). The modifiable areal unit problem, Geo Abstracts University of East Anglia.

Saberi, M., Mahmassani, H. S. and Director, T. C. (2014). Exploring area-wide dynamics of pedestrian crowds using a three-dimensional approach, *Transportation Research Board 93rd Annual Meeting*, number 14-1609.

Steffen, B. and Seyfried, A. (2010). Methods for measuring pedestrian density, flow, speed and direction with minimal scatter, *Physica A: Statistical mechanics and its applications* **389**(9): 1902–1910.

Treiber, M. and Kesting, A. (2013). Traffic flow dynamics, *Traffic Flow Dynamics: Data, Models and Simulation, Springer-Verlag Berlin Heidelberg* .

van Wageningen-Kessels, F., Hoogendoorn, S. P. and Daamen, W. (2014). Extension of edie's definitions for pedestrian dynamics, *Transportation Research Procedia* **2**: 507–512.

Weidmann, U. (1993). Transporttechnik der fussgänger, *Technical Report Schriftenreihe des IVT Nr. 90*, Institut für Verkehrsplanung,Transporttechnik,Strassen- und Eisenbahnbau, ETH Zürich. (In German).

Zhang, J. (2012). *Pedestrian fundamental diagrams: Comparative analysis of experiments in different geometries*, PhD thesis, Forschungszentrum Jülich.